Host-pathogen dynamics in fungal diseases: Comparing SI and multi-infection models

Noam Ross

December 18, 2014

Introduction

Emerging fungal infections pose major threats to plant and animal wildlife populations as well has livestock and crops, as do oomycetes, which have similar life-histories to fungi. These common life history traits, including high virulence, long-lived environmental reservoirs, and host generalism are thought to contribute to the potential of these pathogens to drive local and global extinctions of some species (Fisher et al. 2012, Eskew and Todd 2013).

An important component fungal host-pathogen dynamics is the role of spore load in driving host infection and mortality. Briggs et al. (2010) showed that population-level persistence or extinction of mountain yellow-legged frogs (*R. sierrae*) infected by chytrid fungus (*Batrachochytrium dendrobatidis*), could be explained by the dynamics of spore load build-up in these populations. Similarly, mortality of bat populations with White Nose Syndrome (*Geomyces destructans*) is closely related to spore load on bat skin, which builds up through bat-to-bat contact over the course of the hibernation period (Langwig et al. 2015). The fungal parasite *Metschnikowia bicuspidata* kills its *Daphnia* host when the parasite loads are high enough to interfere with cell metabolism (Hall et al. 2009). Many mammals, including humans, which are generally resistant to fungal diseases or asymptotic under normal conditions may nonetheless become infected and exhibit symptoms or mortality under persistent exposure to large fungal spore loads (Casadevall 2005).

Many plant diseases also present as an accumulation of local infections, rather than systemic infections, and this has long been recognized as an important component of plant disease dynamics (Waggoner and Rich 1981, Dobson and Crawley 1994, McRoberts et al. 2003), especially in cases of parasitic plants such as mistletoe (Martinez and Effects 1996). Sudden Oak Death, caused by the oomycete *Phyophthora ramorum*, kills tanoak (*Notholithocarpus densiflorus*) faster in the presence of large numbers of other infected hosts, indicating that continued accumulation of infections, rather than just disease progress, drives mortality (Cobb et al. 2012).

Most attempts to model fungal disease dynamics have used various modifications of tradition susceptible-infected (*SI*) disease frameworks, which represent disease as a binary state of the host. Extensions such as susceptible-exposed-infected-removed (*SEIR*) models represent disease progression within hosts, but do not capture the accumulation of *new* infections that may drive disease impacts. This dynamic may be better captured using the framework created by Anderson and May (1978) to model macroparasite infections, where disease is represented as an indefinite number of discrete infections (or parasites), within each host. Here I use the term multi-infection to describe these models.

Age and stage structure is another potentially important factor driving fungal disease dynamics. The effect of Chytrid fungus on frogs varies across life stages (Rachowicz and Vredenburg 2004, Garner et al. 2009). Mortality rates in tanoak are much greater in large trees than small ones (Cobb et al. 2012). However as organisms can grow over similar time scales as the progress of a fungal epidemic, observed patterns in age-disease relationships can be difficult to disentangle from host-pathogen dynamics.

There is a considerable literature on host-pathogen dynamics of in age- and stage-structured populations using *SI* models (Castillo-Chavez et al. 1989, Diekmann et al. 1990, Busenberg and Hadeler 1990, Hethcote 2000, Dietz and Heesterbeek 2002, Klepac and Caswell 2010). There is a somewhat smaller literature on disease in multi-infecton models, especially in cases where host populations vary on the same time scale as the disease. In multi-infection models, Krasnov et al. (2006) showed that parasite counts increase with age in rodents. Pacala and Dobson (1988) created a method to detect the mortality effect of macroparasites

based of the distribution of parasites among different age groups. Duerr et al. (2003) showed how a age-infection relationships could be modified by a variety of age- time- and density-dependent processes, but also showed that interpretation of such age-infection patterns was ambiguous if more than one such process was operating.

Response to disease outbreak often requires prediction of medium- and long-term behavior from early-phase dynamics of disease, which in turn requires mechanistic disease models. However, in early stages of epidemics of emerging diseases, the importance of disease load may not be known, nor the appropriateness of multi-infection rather than *SI* models. Disease load is often considerably more difficult to measure than prevalence, allowing only observations of susceptible vs. infected states. However, model choice may have considerable influence on predictions of disease dynamics and management response.

Here I explore how host-pathogen dynamics differ between *SI* and multi-infection models. I examine how *SI* and multi-infections models differ long-term dynamics when parameterized to fit identical short-term conditions, and vice versa. I also explore how patterns of disease across life stages differ between over the course of epidemics in *SI* and multi-infection models.

Methods

Model Structure

I compared dynamics in 3 ODE-based disease models: A simple SI model, a multi-infection model based on Anderson and May (1978), and an intermediate SIV (susceptible-infected-*very* infected) model.

Each model has a two-stage population structure (population N = juveniles J + adults A). New individuals enter the uninfected, juvenile stage via density-dependent recruitment ($fN(1-N/K)$, where f is fecunidity and K carrying capacity). Individuals move from juvenile to adult classes at the transition rate g.

Disease transmission is density-dependent; susceptible individuals (J_S, A_S) become infected (J_I, A_I) at a rate equal to the density of other infected individuals times the transmissivity of the disease (λ). All individuals die at the a base rate (d), and diseased individuals have additional mortality (α)

The complete SI model is

$$\begin{aligned}
\frac{dJ_S}{dt} &= fN(1-N/K) - J_S(d+g+\lambda J_I + \lambda A_I) & \frac{dA_S}{dt} &= gJ_S - A_S(d+\lambda N) \\
\frac{dJ_I}{dt} &= \lambda J_S(J_I+A_I) - J_I(d+g+\alpha) & \frac{dA_I}{dt} &= gJ_I + \lambda A_S(J_I+A_I) - A_I(d+\alpha) \\
N &= J_S + A_S + J_I + A_I
\end{aligned}$$

Note that this is a *null model* of age structure; neither demographic nor epidemiological parameters vary with age. When juvenile and adult classes are summed, the growth term g drops out, and dN/dt is independent of g.

The other two models are extensions of the SI model with additional disease classes representing degrees of infection. In the multi-infection model, there are an infinite number of disease classes designated $i = 0, 1, 2, \ldots, \infty$. For purposes of simulation, the number of classes is truncated, with a maximum value of k. Transmissivity (λ) and mortality (α) and are additive in these models, increasing linearly with i. Trees advance to the next disease class at rate Λ, the overall force of infection, which is the sum of each tree's contribution, $i\lambda$. Trees in each stage die at rate $d + i\alpha$. Here is the complete multi-infection model:

$$\frac{dJ_0}{dt} = fN(1-N/K) - J_0(d+g+\Lambda) \qquad \frac{dA_0}{dt} = gJ_0 - A_0(d+\Lambda)$$
$$\frac{dJ_i}{dt} = \Lambda dJ_{i-1} - J_i(d+g+i\alpha+\Lambda) \qquad \frac{dA_i}{dt} = gJ_i + \Lambda A_{i-1} - A_i(d+i\alpha+\Lambda)$$
$$\frac{dJ_k}{dt} = \Lambda dJ_{k-1} - J_k(d+g+k\alpha) \qquad \frac{dA_k}{dt} = gJ_k + \Lambda A_{k-1} - A_k(d+k\alpha)$$
$$N = \sum_{i=0}^{k} J_0 + A_0 \qquad \Lambda = \lambda \sum_{i=1}^{k} i(J_i + A_i)$$

The SIV model is merely a truncated version of the multi-infection model, with $k = 2$. For this model I refer N_0 as S, N_1 as I and N_2 as V, and use S, I, and V, as subscripts for J, and A as well.

In this paper, parameters (e.g., λ and α) are subscripted with param_{SI}, param_{SIV}, or $\text{param}_{\text{multi}}$ when referring to their values in each of the three models. I also use the term "infected" to refer to individuals of either the I class in the SI model, or having at least one infection in the SIV or multi-infection models.

Multi-infection models typically assume a distribution of infections in order to reduce the system of equations (Anderson and May 1978). Negative-binomial distributions of infections allow tractable analysis of such models and match empirical studies of infection distribution in the wild (Wilson et al. 2002). However, the reduced model only approximates the full model asymptotically (Adler and Kretzschmar 1992), and key assumptions of the reduced model break down in the presence of age structure (See Appendix.) Instead, I avoided making such assumptions by simulating the the infinite system of equations truncating at k.

Comparative parameterization

I compared the models' behaviors under "equivalent" parameterizations. As the models have different structures, their parameters in the models have different interpretations. Specifically, λ and α operate on a per-individual basis in the SI model, while they operate on a per-infection basis on the SIV and multi-infection models. Thus, they are not *identical* parameterizations.

In order to determine equivalent parameterizations between models, I set parameters for the SI model to those in Table 1. I then fit the SIV and multi-infection models so that they would exhibit identical *behavior* to the SI model under different criteria. The behavior of SIV and multi-infection models were adjusted by multiplying both the infectivity ($\lambda_{SIV}, \lambda_{multi}$) and disease-induced mortality ($\alpha_{SIV}, \alpha_{multi}$) parameters by a constant c. Where there there were dual behavior criteria (behaviors (4) and (5) below), the λ and α values were allowed to vary independently.

Initial conditions in simulations were set at the disease-free equilibrium of the system, modified with 1% of both juveniles and adults having a single infection.

Parameter	Symbol	Base Case Value
fecundity	f	1
carrying capacity	K	1
transition rate	g	0.1
mortality	d	0.01
disease-induced mortality	α	0.2
transmissivity	λ	3
max number of infections (SIV/multi-infection)	k	3 / 150

Table 1: Base parameters for disease models

I examined model behavior in three cases.

1. **Equilibrium mortality rate**. The first behavioral criterion was identical equilibrium mortality rate across models. c was varied to match the overall disease-induced mortality rate (and thus the total mortality rate) between models. That is, at steady state,

$$\alpha_{SI} = \alpha_{SIV}\frac{I+2V}{I+V} = \alpha_{\text{multi}}\frac{1}{N}\sum_i iN_i$$

2. **Initial growth and acceleration rates of infected individuals.** Next, c was adjusted such that the first and second derivatives of growth of total infected individuals under initial conditions. That is,

$$\frac{dI}{dt} = \frac{d(I+V)}{dt} = \frac{dN_{i>0}}{dt}, \text{ and}$$
$$\frac{d^2I}{dt^2} = \frac{d^2(I+V)}{dt^2} = \frac{d^2N_{i>0}}{dt^2}$$

at initial conditions of $S \approx N$, $I_{SI} = I_{SIV} = N_{1\,multi} \approx 0$ and $I_{SIV} = N_{i\geq 2\,multi} = 0$.

Note that the first condition, of the initial growth rate of infected individuals, is identical at all cases under these initial conditions. Thus, I used only the second derivative to fit parameter values.

3. **Time to 10% infection**. This criterion was selected to match behavior among models during the early transient period of disease. c was adjusted so that the SIV and multi-infection models would reach 10% infection in the same time period as the SI model. That is,

$$t\big|_{\frac{I}{S+I}=0.1} = t\big|_{\frac{I+V}{S+I+V}=0.1} = t\big|_{\frac{N_{i\geq 1}}{N}=0.1}$$

All simulations simulations were performed in R (R Core Team 2014), using the deSolve package (Soetaert et al. (2010)) for simulation, the numDeriv package to determine derivatives (Gilbert and Varadhan (2012)), and the ggplot2 (Wickham (2009)) package for plotting. Code to reproduce these results is archived online (**???**).

Results

Aggregate dynamics

Models with similar equilibrium behavior differ in initial transient behavior. Figure 1 shows the dynamic behavior of the SI, SIV, and multi-infection models calibrated to equivalent mortality at equilibrium. Under this parameterization, all models reach an internal equilibrium with a population level suppressed from the disease-free equilibrium at which they started. As all other rates are equal, the equilibrium populations are identical between the models, as well.

Under this parameterization, the ratio of α and λ values between the models (c) is the inverse of the mean number of infections at equilibrium in the SIV and multi-infection models. This value is 0.69 for the SIV model and 0.61 for the multi-infection model.

In the SIV and multi-infection models, the apparent mortality rate of infected individuals increases over time. Early in the epidemic, individuals have small numbers of infections, thus the mortality rate across individuals with any level of infection is low. As the epidemic progresses, the mean number of infections per infected individual increases, raising the mortality rate of the infected class until equilibrium is reached.

The change in mortality rates is driven by changes in the distribution of infections over time, shown in Figures 2 and 3. As the disease progresses through the population in the SIV model, the proportion of individuals in the I and V classes increases for both juveniles and adults. Similarly, in the multi-infection model, the mean number of infections in each individual increases over time, increasing the mortality rate.

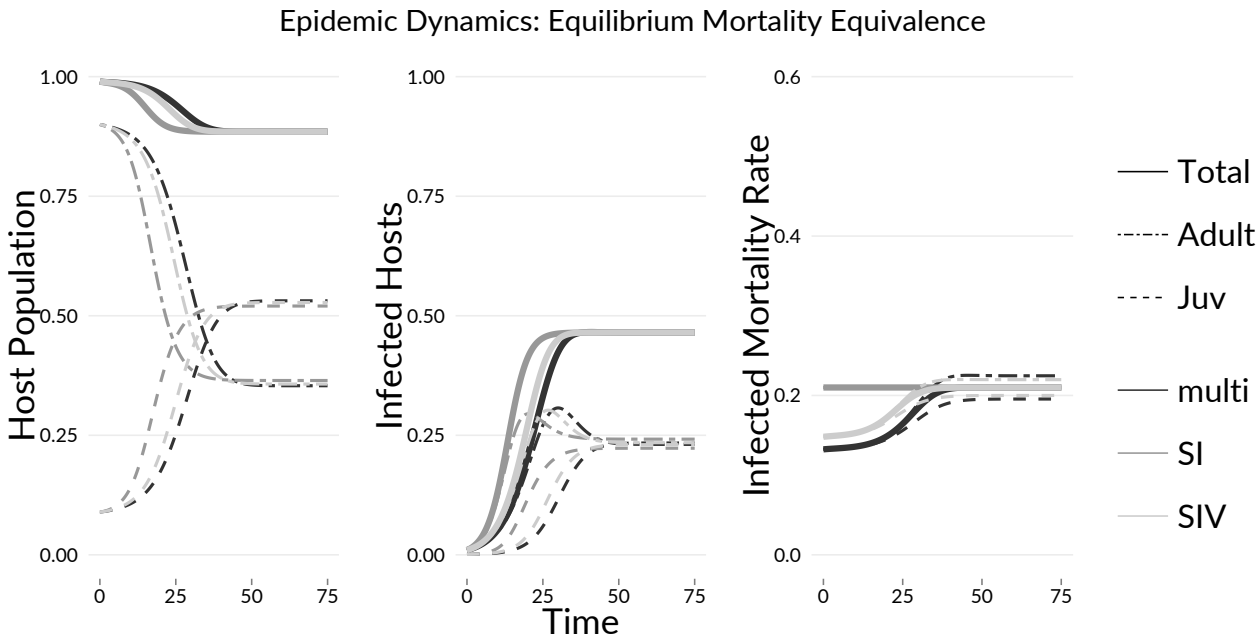

Figure 1: Figure 1: Dynamics of models parameterized to equivalent equilibrium mortality rates

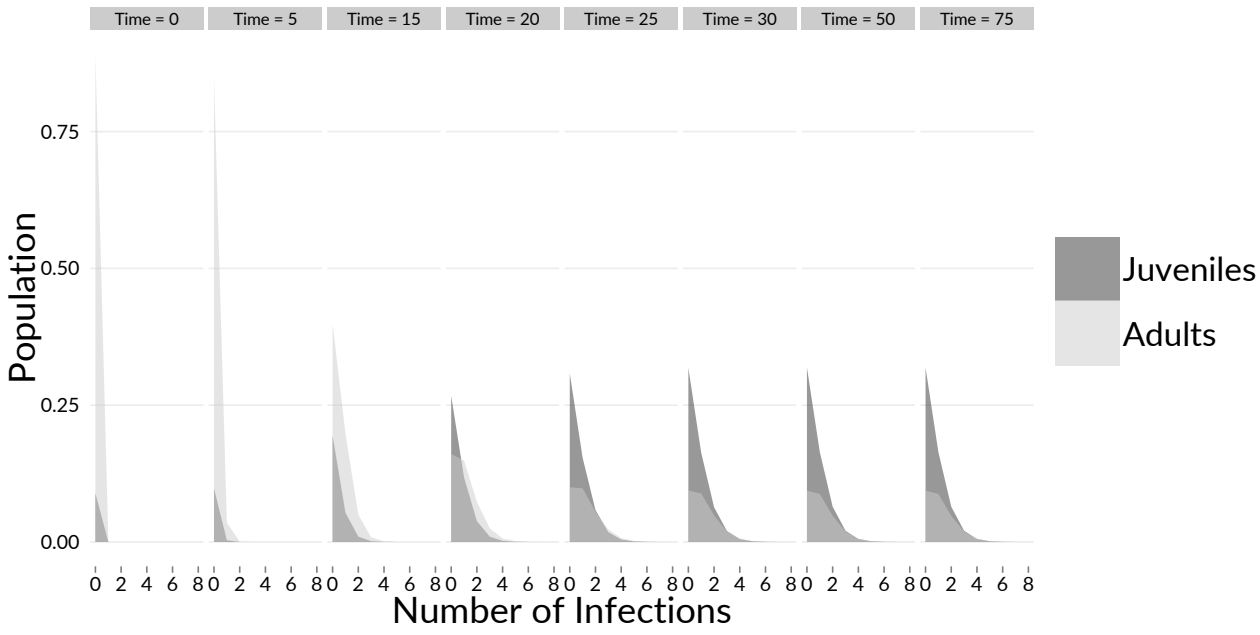

Figure 2: Figure 2: Dynamics infection classes in the SIV model

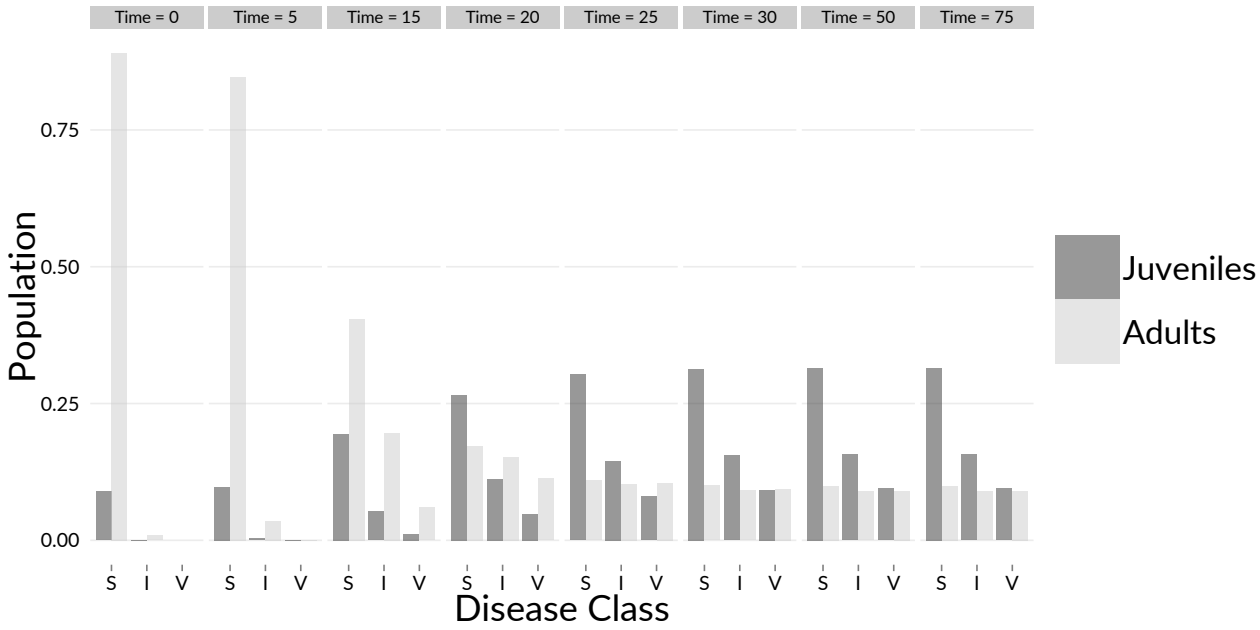

Figure 3: Figure 3: Dynamics of infection classes in the multi-infection model

While equilibrium behaviors are identical and models start at the same initial conditions, transient behavior differs. The time to equilibrium is greater in the multi-infection model than the SIV model, and greater in both than the SI model. It takes longer in the SIV model, and longest in the multi-infection model, for the disease to emerge.

Models with similar initial behavior reach different equilibrium conditions. Figure 4 shows the dynamics of the three models in the case where the initial first and second derivatives are equivalent. As in the matching-equilibrium parameterizations, mortality for infected individuals increases over time until equilibrium is reached. Unlike that parameterization, per-infection parameters in the SIV/multi-infection models (mortality and infectivity), are similar to per-individual parameters in the SI model. c is 0.99 for the SIV model and 0.99 for the multi-infection model. Total mortality rates for the SIV and multi-infection models start at the same levels as the SI model and diverge over time.

The SIV and multi-infection models have nearly identical behavior. At equilibrium, their populations are suppressed to lower levels than in the SI model, and a smaller number of the individuals are infected. This is because the difference in mortality rates of infected individuals between the SI and the other models is greater, increasing turnover of infected individuals. In this case, the SIV and multi-infection models reach equilibrium *before* the SI model.

Figure 5 shows model dynamics when models were parameterized to have equivalent timeuntil 10% of the total population was infected. As with the last parameterization, the initial mortality rates of the SIV and multi-infection models are similar to those in the SI model; per-infection parameters in SIV/multi-infection models are similar to per-individual parameters in the SI model. Here c is 0.98 for the SIV model and 0.98 for the multi-infection model.

Patterns in the time-to-10%-infection parameterizations are similar to the matched-second-derivative parameterization. Mortality rates for individuals in SIV and multi-infection models increase before reaching equilibrium, resulting in lower population sizes and lower populations of infected individuals at equilibrium. Dynamics for the SIV and multi-infection models are again very similar, though not as similar as in the matched-derivative case. Also, in this case, the number of infected individuals reaches a peak before going down to reach equilibrium levels.

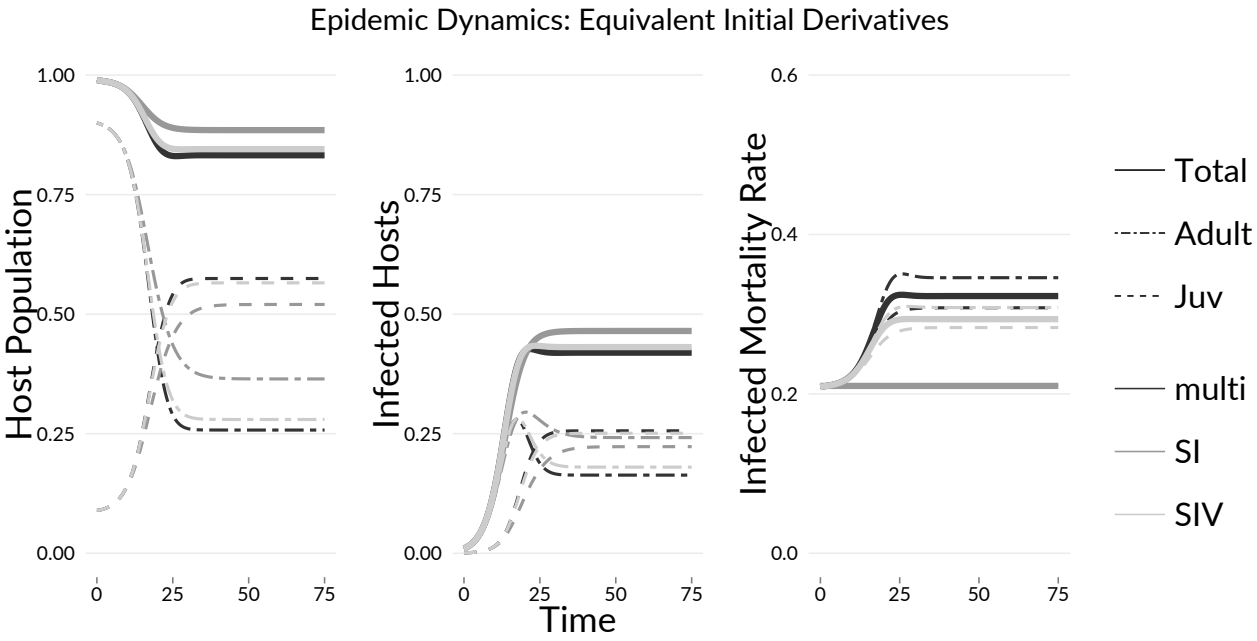

Figure 4: Figure 4: Dynamics of models parameterized to equivalent initial rates of growth of infectious individuals

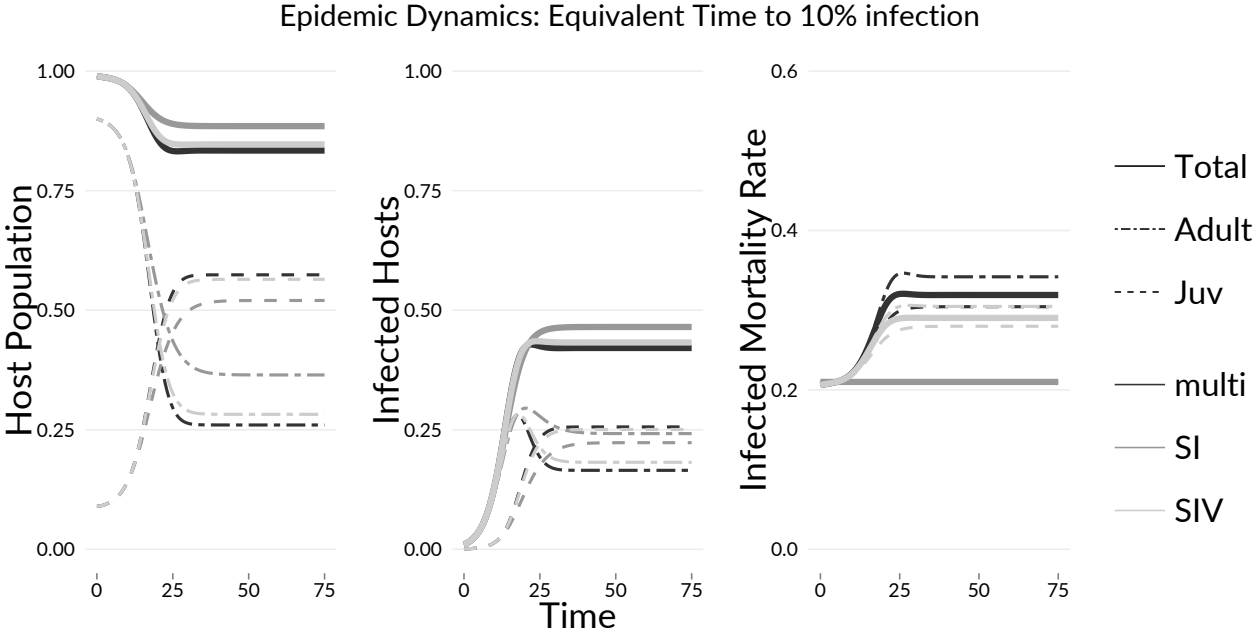

Figure 5: Figure 5: Dynamics of models parameterized to equivalent time to 10% infected individuals

Age effects

Multi-infection models generate age-dependent effects not found in SI models.

All three models, under all three parameterizations, exhibit some common patterns in the dynamics of population stages. From the disease-free equilibrium dominated by adults, disease outbreak decreases the population of adult stages and and increases both the relative and absolute population of the juvenile stages. The infected population of both stages increases, with the adult infected stage reaching a peak before equilibrium and the juvenile infected stage reaching a smaller equilibrium with no peak.

In the equivalent equilibrium mortality parameterization, The SIV and multi-infection stage structures are slower to reach an equilibrium than the SI stage structure, with the multi-infection case being slowest. This is similar to the aggregate dynamics for this parameterization. In the case of equivalent initial derivatives, as will as the case of equivalent time to 10% infection, the change in age structure from the disease-free equilibrium is greater in the SIV and multi-infection models than the SI model. at equilibrium, there are more juveniles and fewer adults in the SIV/multi-infection cases.

In the SIV and multi-infection models, the mortality rate of infected juveniles and adults increases as the disease progresses, and their mortality rate diverges, with adults having greater mortality rates than juveniles at equilibrium. This occurs in all parameterizations. The reason for this can be found in figures 2 and 3, which show the distribution of infections for both adult and juvenile populations over the course of the epidemic in SIV and multi-infection models. Adults and juveniles begin with equal mean numbers of infections, but as the epidemic continues, adult trees accumulate more infections than juveniles by both new infections on adult trees and already-infected juveniles recruiting into the adult population.

In a multi-infection model with age structure, individuals accumulate infections over time, resulting in more infections, and thus greater mortality and infectivity, among older individuals than younger individuals. Even in the absence of age-driven variation in how individuals respond to disease (that is, in a "null model"), different behavior is observed between age groups. In an SI model, these differences do not arise.

Discussion

SI and multi-infection models represent disease different ways: as binary states of an individual, or as accumulations of multiple infections across individuals. As a result, they may produce different host-pathogen dynamics. The choice of model structure has important consequences for the prediction of host-pathogen disease dynamics.

Epidemics that appear to be well represented by SI models during their outbreak phase may no longer be well represented in later stages if they have dynamics driven by multiple infections. A multi-infection model that behaves like an SI model in early stages will diverge from SI behavior as increasing infection loads result in greater per-individual mortality rates. I found similar behavior regardless of the criterion used to determine early-phase dynamics (derivatives or time-to-10%-infection). If the multi-infection system system has an equilibrium (other than disease-free or extinction), the host population will be lower at this equilibrium than in an SI system due to greater suppression from to disease, while the diseased population itself will be lower as highly infected individuals suppressing population more. A *smaller* fraction of the population will be infected at equilibrium, because of the short survival of highly infected individuals.

I found similar patterns in the reverse case, where early disease behavior was predicted from equilibrium behavior using both SI and multiple-infection models. Multiple-infection models with the same equilibrium behavior as SI models are slower to emerge, as the small numbers of infections on initially infected individuals transmit less disease and kill at slower rates than "fully" infected individuals in the SI model, which have higher per-individual transmission mortality. The models converge when mean infection numbers in individuals in the multi-infection model rise such that their virulence matches individuals in the SI model.

Multiple-infection models indicate that age- or stage-related patterns in disease mortality can arise from the accumulation of infections over time, even in the absence of biological differences among age class in susceptibility to disease. Here I found that, in all parameterizations of multi-infection models, adult mortality rates

increased faster than juvenile mortality rates as epidemics progressed, even though per-infection mortality rates were identical between life stages. While in some fungal diseases, host-pathogen interactions drive differences in virulence between life stages (e.g., chytrid fungus, see Rachowicz and Vredenburg (2004)), this difference could explain part or all of stage-related differences in mortality in fungal diseases, such as in Sudden Oak Death (Cobb et al. 2012).

Multiple infection-models also showed increase population-level age effects of disease. In simulations where both SI and multi-infection models had similar initial behavior, disease resulted in a shift from adult- to juvenile dominance over the course of the epidemic, but in the multiple-infection model this shift was greater, as adult mortality was greater. Also, adult disease prevalence was lower in the late stages of multiple infection models, because with higher adult mortality diseased adults have short lifespans.

Simplified models of multiple infection, such as the SIV model presented here, can capture some of the components of load-driven disease dynamics. Here, the SIV model behaved similarly to the multi-infection model, including similar differences in time-to-equilibrium from the SI model, similar suppression of the final population, similar total infected host number, and age-mortality patterns. However, there were differences between the SIV and multi-infection model in the apparent mortality rate of infected hosts, especially in the time-to-10%-infection parameterization, indicating a role of the long tail of hosts with high infection number in driving this pattern.

These results indicate that identifying multi-infection driven diseases early in their emergence will significantly alter predictions of disease dynamics. Can the dynamics of these disease be distinguished from those of SI-like processes in the data from early-stage emerging epidemics, especially when data are of disease prevalence rather than load? One way to distinguish these mechanisms is to look for changes in mortality rate as disease progresses or between early- or late-period populations, or to look for differences in mortality rate among age classes. Both these patterns can indicate multi-infection-driven processes. However, similar to what Duerr et al. (2003) demonstrated, such patterns are not sufficient to disentangle the multiple processe that may drive mortality patterns. Direct measurements relationships between infection load and host effects are needed to establish the role of multi-infection processes.

References

Adler, F. R., and M. Kretzschmar. 1992. Aggregation and stability in parasite—host models. Parasitology 104:199–205.

Anderson, R., and R. May. 1978. Regulation and stability of host-parasite population interactions: I. Regulatory processes. The Journal of Animal Ecology 47:219–247.

Briggs, C. J., R. a Knapp, and V. T. Vredenburg. 2010. Enzootic and epizootic dynamics of the chytrid fungal pathogen of amphibians. Proceedings of the National Academy of Sciences of the United States of America 107:9695–700.

Busenberg, S. N., and K. Hadeler. 1990. Demography and epidemics. Mathematical Biosciences 101:63–74.

Casadevall, A. 2005. Fungal virulence, vertebrate endothermy, and dinosaur extinction: is there a connection? Fungal genetics and biology : FG & B 42:98–106.

Castillo-Chavez, C., H. W. Hethcote, V. Andreasen, S. A. Levin, and W. M. Liu. 1989. Epidemiological models with age structure, proportionate mixing, and cross-immunity. Journal of Mathematical Biology 27:233–258.

Cobb, R. C., J. A. N. Filipe, R. K. Meentemeyer, C. A. Gilligan, and D. M. Rizzo. 2012. Ecosystem transformation by emerging infectious disease: loss of large tanoak from California forests. Journal of Ecology 100:712–722.

Diekmann, O., J. Heesterbeek, and J. Metz. 1990. On the definition and the computation of the basic reproduction ratio R 0 in models for infectious diseases in heterogeneous populations. Journal of Mathematical Biology 28:365–382.

Dietz, K., and J. Heesterbeek. 2002. Daniel Bernoulli's epidemiological model revisited. Mathematical Biosciences 180:1–21.

Dobson, A., and M. Crawley. 1994. Pathogens and the structure of plant communities. Trends in Ecology & Evolution 9:393–8.

Duerr, H. P., K. Dietz, and M. Eichner. 2003. On the interpretation of age–intensity profiles and dispersion patterns in parasitological surveys. Parasitology 126:87–101.

Eskew, E. A., and B. D. Todd. 2013. Parallels in Amphibian and Bat Declines from Pathogenic Fungi. Emerging Infectious Diseases 19:379–385.

Fisher, M. C., D. a Henk, C. J. Briggs, J. S. Brownstein, L. C. Madoff, S. L. McCraw, and S. J. Gurr. 2012. Emerging fungal threats to animal, plant and ecosystem health. Nature 484:186–94.

Garner, T. W. J., S. Walker, J. Bosch, S. Leech, J. Marcus Rowcliffe, A. a. Cunningham, and M. C. Fisher. 2009. Life history tradeoffs influence mortality associated with the amphibian pathogen Batrachochytrium dendrobatidis. Oikos 118:783–791.

Gilbert, P., and R. Varadhan. 2012. numDeriv: Accurate Numerical Derivatives.

Hall, S. R., J. L. Simonis, R. M. Nisbet, A. J. Tessier, and C. E. Cáceres. 2009. Resource ecology of virulence in a planktonic host-parasite system: an explanation using dynamic energy budgets. The American Naturalist 174:149–62.

Hethcote, H. W. 2000. The Mathematics of Infectious Diseases. SIAM Review 42:599–653.

Klepac, P., and H. Caswell. 2010. The stage-structured epidemic: linking disease and demography with a multi-state matrix approach model. Theoretical Ecology 4:301–319.

Krasnov, B. R., M. Stanko, and S. Morand. 2006. Age-dependent flea (Siphonaptera) parasitism in rodents: a host's life history matters. The Journal of Parasitology 92:242–8.

Langwig, K. E., W. F. Frick, R. Reynolds, K. L. Parise, K. P. Drees, J. R. Hoyt, T. L. Cheng, T. H. Kunz, J. T. Foster, and a M. Kilpatrick. 2015. Host and pathogen ecology drive the seasonal dynamics of a fungal disease, white-nose syndrome. Proceedings. Biological sciences / The Royal Society 282:10–12.

Martinez, C., and C. Effects. 1996. Effects of the mistletoe Tristerix on the aphyllus reproduction of its cactus host Echinopsis chilensis 3:437–442.

McRoberts, N., L. V. Hughes, G, and L. V. Madden. 2003. The theoretical basis and practical application of relationships between different disease intensity measurements in plants. Annals of Applied Biology 142:191–211.

Pacala, S. W., and A. P. Dobson. 1988. The relation between the number of parasites/host and host age: population dynamic causes and maximum likelihood estimation. Parasitology 96:197.

R Core Team. 2014. R: A Language and Environment for Statistical Computing. R Foundation for Statistical Computing, Vienna, Austria.

Rachowicz, L. J., and V. T. Vredenburg. 2004. Transmission of Batrachochytrium dendrobatidis within and between amphibian life stages. Diseases of Aquatic Organisms 61:75–83.

Soetaert, K., T. Petzoldt, and R. W. Setzer. 2010. Solving Differential Equations in R: Package deSolve. Journal of Statistical Software 33:1–25.

Waggoner, P. E., and S. Rich. 1981. Lesion distribution, multiple infection, and the logistic increase of plant disease. Proceedings of the National Academy of Sciences of the United States of America 78:3292–5.

Wickham, H. 2009. Ggplot2. Springer New York, New York, NY.

Wilson, K., O. N. Bjørnstad, A. P. Dobson, S. Merler, G. Poglayen, A. F. Read, and A. Skorping. 2002. Heterogeneities in macroparasite infections: patterns and processes. Pages 6–44 *in* The ecology of wildlife diseases.